Journal of Power Sources 248 (2014) 122–129

Contents lists available at ScienceDirect

Journal of Power Sources

journal homepage: www.elsevier.com/locate/jpowsour

Electrochemical characteristics of lithium vanadate, Li_3VO_4 as a new sort of anode material for Li-ion batteries

Shibing Ni, Xiaohu Lv, Jianjun Ma, Xuelin Yang*, Lulu Zhang

College of Mechanical and Material Engineering, Three Gorges University, 8 Daxue Road, Yichang 443002, PR China

HIGHLIGHTS

- We firstly researched the electrochemical performance of Li_3VO_4 as anode for Li-ion battery.
- We discussed the possible charge/discharge mechanism of Li_3VO_4.
- The Li_3VO_4 anode shows excellent cycle stability and rate capability.
- We found a lithium ion diffusion controlled mechanism for the Li_3VO_4 anode.

GRAPHICAL ABSTRACT

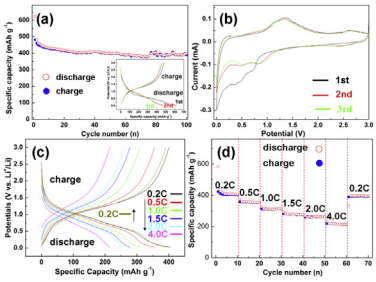

ARTICLE INFO

Article history:
Received 28 July 2013
Received in revised form
29 August 2013
Accepted 13 September 2013
Available online 20 September 2013

Keywords:
Electrochemical performance
Lithium ion battery
Redox reaction mechanism
Vanadium element based transition metal oxides

ABSTRACT

Li_3VO_4 is fabricated by a facile hydrothermal method and subsequent annealing treatment. The electrochemical performance and the possible charge/discharge mechanism of the as-prepared Li_3VO_4 as anode for Li-ion battery are firstly studied. Galvanostatic battery testing shows that the Li_3VO_4 electrode exhibits excellent cycle stability and rate capability. At a current density of 0.25 C, it delivers initial discharge and charge capacity about 624 and 481 mAh g^{-1}, respectively, which maintains of 398 and 396 mAh g^{-1} after 100 cycles. After 60 cycles at various rates from 0.2 to 4.0 C, the discharge capacity can restore 98% when lowering the charge/discharge rate to 0.2 C. A possible redox reaction mechanism is proposed to interpret the lithiation/delithiation process of Li_3VO_4 according to experimental observations. The electrochemical reaction kinetic of the Li_3VO_4 electrode is studied by cyclic voltammetry measurement at various scan rate, which indicates the anodic and cathodic peak currents show linear dependence on the square root of scan rate from 0.3 to 1.0 mV s^{-1}, suggesting a lithium ion diffusion controlled mechanism in the charge/discharge process.

1. Introduction

Li-ion batteries are becoming not only the main power source in today's portable electronic devices but also the potential power sources of electric vehicles and hybrid electric vehicles. One of the key issues in the development of Li-ion batteries is to explore electrode materials with higher capacity and better electrochemical performance.

Transition metal oxides (TMOS) become promising anode candidates for Li-ion batteries owing to their high theoretical capacity (500–1000 mAh g^{-1}) that based on a novel redox reaction [1]. Various kinds of TMOS such as Fe_3O_4, Fe_2O_3, Co_3O_4, CoO, NiO and Cu_xO ($x = 1, 2$) as anodes for Li-ion battery have been extensively researched by now [2–7], which shows impressive electrochemical performance. As one sort of specific TMOS, vanadium oxides (V_xO_y) usually show layered or channel-like structure, undergoing an intercalation/deintercalation reaction mechanism for lithium ions storage and usually acting as cathode materials for Li-ion batteries [8–12]. The introduction of metal element (Fe, Cu, Zn etc.) into vanadium oxides has resulted in the emergence of many sorts of

* Corresponding author. Fax: +86 717 6397559.
E-mail addresses: shibingni07@gmail.com (S. Ni), xlyang@ctgu.edu.cn (X. Yang).

0378-7753/$ – see front matter © 2013 Elsevier B.V. All rights reserved.
http://dx.doi.org/10.1016/j.jpowsour.2013.09.050

new ternary compounds, which exhibit enticing electrochemical properties owing to their peculiar structures. Different kinds of vanadium element based TMOS (TVOS) such as ZnV_2O_4, $FeVO_4$, ZnV_2O_6, CuV_2O_6, $Cu_2V_2O_7$, $Cu_5V_2O_{10}$ and $Ag_2V_4O_{11}$ have been fabricated and their electrochemical performance were studied [13–17], which show much different electrochemical characteristics. For example, ZnV_2O_4 and $FeVO_4$ exhibit relative low voltage versus Li metal, suggesting them as potential anode materials for Li-ion batteries, whereas ZnV_2O_6, CuV_2O_6, $Cu_2V_2O_7$, $Cu_5V_2O_{10}$ and $Ag_2V_4O_{11}$ exhibit relative high voltage versus Li, suggesting them as potential cathode materials for Li-ion batteries. Such difference comes from the diverse crystal structure of TVOS that determined by the multiform valence values of vanadium and transition metal elements. TVOS usually undergo complex electrochemical reactions during the charge and discharge process, resulting in interesting electrochemical behavior. Fox example, $Ag_2V_4O_{11}$ undergoes the reduction of V^{5+}, the displacement between Li^+ and Ag^+, the structure collapse, the reduction of Ag^+ and the reduction of V^{4+} during the discharge process, and the re-enter of Ag without recovering the original crystal structure during the charge process [17]. Nevertheless, the fabrication of new sort of TVOS and optimization their electrochemical performance is desirable for the development of Li-ion batteries. Introducing of light metal elements in TVOS may be beneficial to improve the specific capacity due to the reduced molecular weight, and Li spontaneously becomes an ideal candidate element. Li element contained TVOS (LVOS) such as $Li_{1+x}VO_2$, LiV_3O_8, $LiVO_3$ and LiV_2O_5 have already shown attractive electrochemical performance [18–21], and the research on the electrochemical property of new sort of LVOS will undoubtedly bring us new surprise in electrochemical field. Here in this paper, we report the preparation of Li_3VO_4 and its electrochemical performance as anode material for Li-ion batteries. The main objective of this paper is to explore the electrochemical performance of Li_3VO_4 as anode for Li-ion battery and the possible charge/discharge mechanism, which may be benefit to further study on improving the electrochemical performance of Li_3VO_4.

2. Experimental section

2.1. Fabrication procedure

The chemicals were analytical grade and purchased from Shanghai Chemical Reagents. In a typical procedure, 1 mmol V_2O_5, 3 mmol Li_2CO_3 and 5 mmol hexamethylenetetramine were dissolved in 30 ml distilled water. After stirring for 20 min, the homogeneous yellowy suspension was transferred into a 50 ml teflonlined autoclave, distilled water was subsequently added to 80% of its capacity. The autoclave was at last sealed and placed in an oven, heated at 120 °C for 24 h. The transparent solution was dried in an oven at 60 °C. After that, the white precipitates were collected and sintered in N_2 atmosphere at 500 °C for 5 h.

2.2. Structure and morphology characterization

The structure and morphology of the resulting products were characterized by X-ray powder diffraction (Rigaku Ultima IV Cu Kα radiation $\lambda = 1.5406$ Å), field-emission scanning electron microscopy (FE-SEM JSM 7500F, JEOL) and transmission electron microscopy (TEM, FEI, Tecnai G2 F30) equipped with selected area electron diffraction (SAED). For the morphology and structure characterization of the electrode after charge and discharge tests, the cell was prized up and the electrode was washed with ethanol and distilled water. The valence state of the sample was studied by X-ray photoelectron spectroscopy (XPS, VG ESCALAB210) using Mg Kα radiation under a pressure of 5×10^{-9} Torr.

2.3. Electrochemical characterization

For fabricating of lithium ion battery, a mixture of 80 wt% of active material, 10 wt% of acetylene black, and 10 wt% of polyvinylidene fluoride (PVDF) dissolved in *N*-methylpyrrolidine (NMP) solution (0.02 g mL^{-1}) were coated on copper foil and cut into disc electrodes with a diameter of 14 mm using a punch. Coin-type cells (2025) of Li/1 M $LiPF_6$ in ethylene carbonate, dimethyl carbonate and diethyl carbonate (EC/DMC/DEC, 1:1:1 v/v/v)/Li_3VO_4 disc electrode were assembled in an argon-filled dry box (MIKROUNA, Super 1220/750, $H_2O < 1.0$ ppm, $O_2 < 1.0$ ppm). A Celgard 2400 microporous polypropylene was used as the separator membrane. The cells were tested in the voltage range between 0.02 and 3 V with a multichannel battery test system (LAND CT2001A). The Cyclic voltammetry (CV) measurement of the electrodes was carried out on a CHI660C electrochemical workstation at a scan rate of 0.2 mV s^{-1} between 0 and 3 V.

3. Results and discussion

Typical XRD pattern of the products is shown in Fig. 1. As seen, the diffraction peaks located at 16.3°, 21.6°, 22.9°, 24.4°, 28.2°, 32.8°, 36.3°, 37.6°, 49.8°, 58.7°, 66.2° and 70.9° can be attributed to the (100), (110), (011), (101), (111), (200), (002), (201), (202), (320), (203) and (322) crystal faces of orthorhombic Li_3VO_4 with lattice constants $a = 6.319$ Å, $b = 5.448$ Å and $c = 4.940$ Å, which is in good agreement with the JCPDS, No. 38-1247. The small diffraction peaks located at 30.4° and 31.6° (marked by *) can be indexed as (311) and (112) crystal faces of orthorhombic V_4O_9 (JCPDS, No. 24-1391).

Fig. 2(a) is a low magnification SEM image of the as-prepared Li_3VO_4, which exhibits porous architecture, consisting of a large number of particles. Fig. 2(b) is a high magnification SEM image of the Li_3VO_4, which indicates the mean size of those particles is about 250 nm. As seen, those particles show smooth surface, among which a large number of holes and interspaces clearly exhibit. TEM provides further insight into the structural details of the Li_3VO_4. As shown in a low magnification TEM image in Fig. 2(c), the Li_3VO_4 particles are composed of nanoparticles with different size ranges from 20 to 100 nm. The insert of Fig. 2(c) is a SAED pattern of the Li_3VO_4 particles, regular diffraction spots suggest the as-synthesized Li_3VO_4 are well crystallized. Fig. 2(d) is a high-resolution TEM (HRTEM) image of the Li_3VO_4, which shows clear lattice fringes. The interplanar spacing is about 0.206 nm, which corresponds to the (220) plane of the orthorhombic Li_3VO_4.

Galvanostatic charge/discharge cycling was carried out in the potential window of 0.02–3.0 V versus Li. Fig. 3(a) is the initial

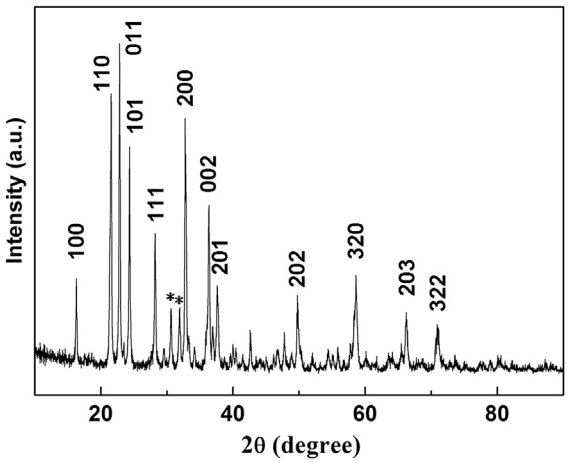

Fig. 1. XRD pattern of the as-prepared products.

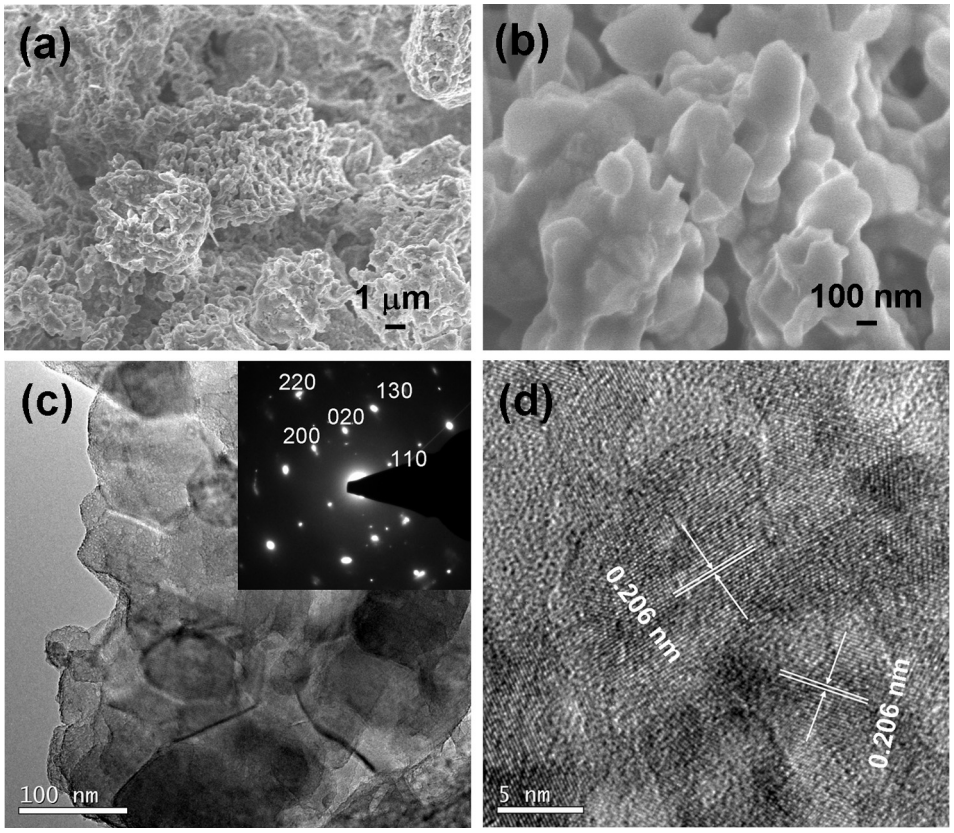

Fig. 2. Low (a) and high (b) magnification SEM images of the as-prepared Li_3VO_4; TEM (c) and HRTEM (d) images of the as-prepared Li_3VO_4. The insert of (c) is a SAED pattern.

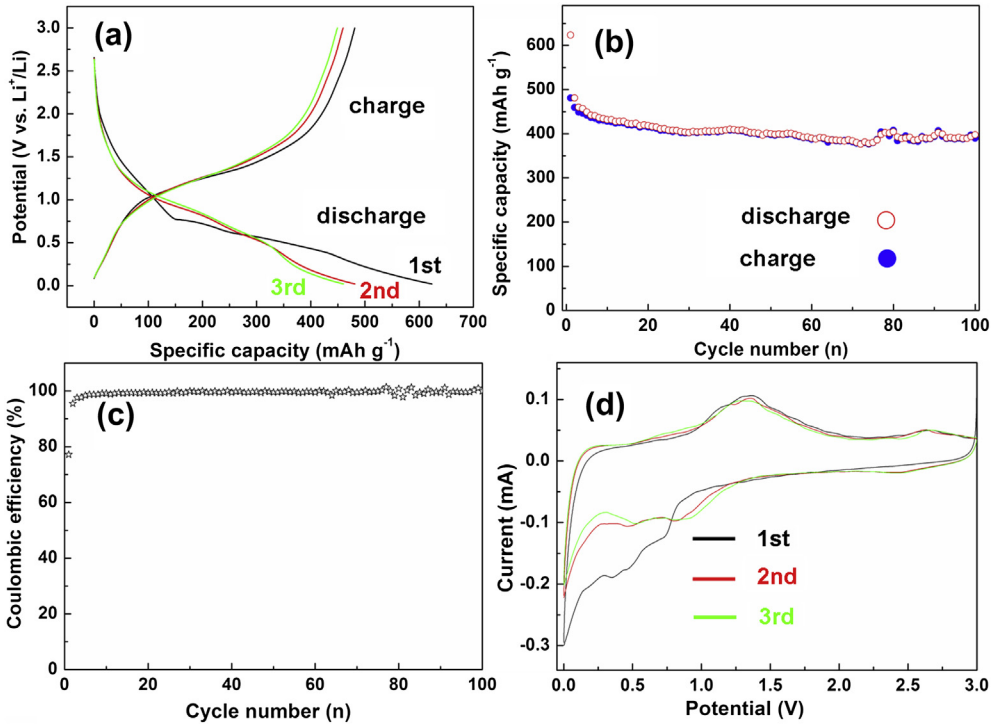

Fig. 3. Electrochemical performance of Li_3VO_4 electrode. (a) The galvanostatic charge/discharge voltage profiles for the initial three cycles. (b) Capacity retention of the galvanostatic test runs at a rate of 0.25 C. (c) Coulombic efficiency. (d) Cyclic voltammograms at a scan rate of 0.2 mV s^{-1}.

three charge and discharge curves at a rate of 0.25 C (1 C means accomplishing discharge or charge in an hour). As seen, the initial discharge curve differs slightly from the 2nd and 3rd one, showing three sloping potential ranges (1.9–0.76, 0.76–0.4 and 0.4–0.02 V) for multistep electrochemical reactions for the lithiation process. The subsequent two discharge curves show two sloping potential ranges (1.9–0.4 and 0.4–0.02 V), accompanied by a decrease of discharge capacity. The initial three charge curves show similar profile with sloping potential range from 0.8 to 1.9 V. Fig. 3(b) shows the capacity retention of the Li_3VO_4 electrode. The initial discharge capacity is 624 mAh g^{-1}, which is bigger than that of the initial charge capacity (481 mAh g^{-1}), corresponding to the irreversible lithium ions consumption during the formation of solid electrolyte interface (SEI). Both the charge and discharge capacity decrease slowly along with the increasing of cycle number in the first few cycles and gradually reach stable values. After 100 cycles, the discharge and charge capacity maintain of 398 and 396 mAh g^{-1}, respectively. The corresponding coulombic efficiency of the Li_3VO_4 electrode is shown in Fig. 3(c). As seen, it exhibits an initial columbic efficiency of 77.2%, which is bigger than traditional TMOS such as Fe_3O_4, NiO and Cu_xO [6,22,23]. The coulombic efficiency increases along with cycle number, being 95.5% and 97.6% in the 2nd and 3rd cycle, respectively. It is noticed that the mean value of coulombic efficiency of the Li_3VO_4 electrode is 99.3% in 100 cycles, which suggests a highly reversible lithiation and delithiation process. The cyclic voltammetric (CV) curves of the Li_3VO_4 electrode were tested over a voltage range from 0 to 3.0 V at a scan rate of 0.2 mV s^{-1}. As shown in Fig. 3(d), the profiles of CV curves of the 2nd and 3rd cycle are similar, whereas an obvious difference between the first and subsequent two cycles is found. In the 1st cathodic scan, two reduction peaks at around 0.41 and 0.74 V are observed, which are attributed to the lithiation process owing to the reduction of Li_3VO_4 and the formation of SEI. The location of the reduction peaks consists well with the voltage plateau in the first discharge curve. The reduction peaks shift to 0.5 and 0.8 V in the 2nd cathodic scan, which can be ascribed to the activation of Li_3VO_4, being similar to TMOS operating conversion mechanism [6,24,25]. In the anodic scan, the oxidation peak locates at about 1.35 V, can be attributed to the delithiation process that involves the reversible formation of Li_3VO_4 and the release of lithium ions.

Fig. 4 is the XRD patterns of the Li_3VO_4 electrode with different discharge and/or charge state. As seen, the diffraction peaks of Li_3VO_4 are clearly observed when discharging to 0.74 V, indicating the lithiation process of Li_3VO_4 doesn't accomplish until discharging to 0.74 V. The diffraction peaks of Li_3VO_4 disappear when further discharging to 0 V, which suggests the reduction

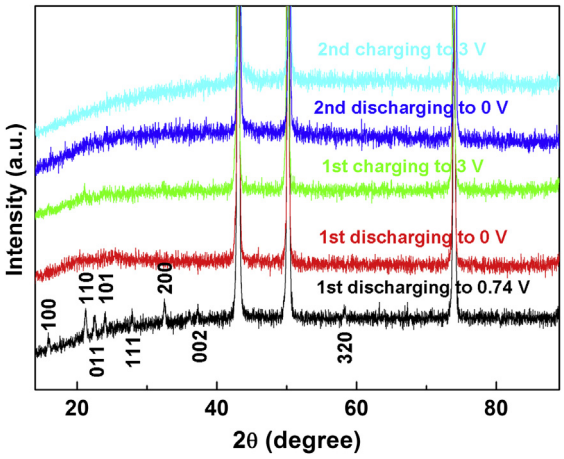

Fig. 4. XRD patterns of Li_3VO_4 under different charge and/or discharge state.

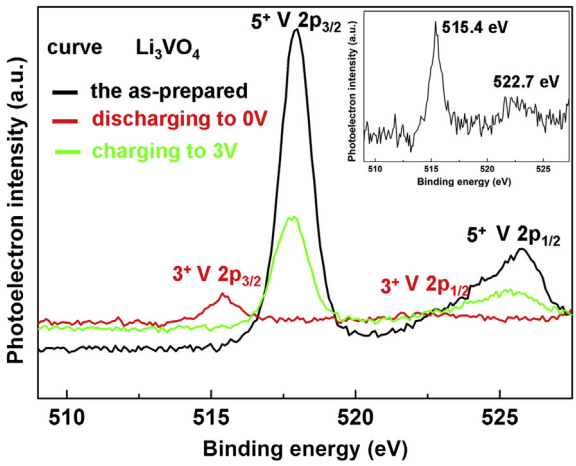

Fig. 5. High resolution XPS spectrum of V 2p region for the as-prepared, full discharged and full charged Li_3VO_4. The insert is the high resolution XPS spectra of V 2p region for the full discharged Li_3VO_4.

of Li_3VO_4 into a new phase. In the first charging process, weak diffraction peaks correspond to (111) and (200) of Li_3VO_4 were detected when charging to 3.0 V, suggesting a reversible redox reaction. In the subsequent charge/discharge process, amorphous state of the electrode is preserved. The observed XRD result is similar to that of NiO possesses redox reaction mechanism [26].

The valence variation of vanadium element with full discharge and charge state was studied by XPS spectra. As shown in Fig. 5, the binding energy of V 2p signals shows clear variation during discharge and charge process. For the as-prepared Li_3VO_4, two peaks located at 517.9 and 525.7 eV can be assigned to the V $2p_{3/2}$ and V $2p_{1/2}$ for V^{5+} [27]. For the Li_3VO_4 electrode discharged to 0 V, two peaks locate at 515.4 and 522.7 eV can be assigned to the V $2p_{3/2}$ and V $2p_{1/2}$ for V^{3+} [27], suggesting the reduction of V^{5+} into V^{3+} in the discharge process. For the Li_3VO_4 electrode charged to 3 V, two peaks of V $2p_{3/2}$ and V $2p_{1/2}$ for V^{5+} at 517.8 and 525.5 eV can be observed again, suggesting the oxidation of V^{3+} into V^{5+} in the charge process. Based on the stable specific capacity of Li_3VO_4 about 400 mAh g^{-1}, it can be deduced that there is about 2 lithium ions contributes to the capacity of a Li_3VO_4 molecular, which accompanies by the reduction and oxidation of V element in Li_3VO_4 in discharge and charge process. Thus we suggest the possible charge/discharge mechanism of Li_3VO_4 is as follows:

$$xLi^+ + Li_3VO_4 + xe^- \rightleftharpoons Li_{3+x}VO_4 (x \leq 2) \quad (1)$$

Further investigation should be done to confirm the detailed lithiation/delithiation behavior of Li_3VO_4, so more effective technique can be adopted to improve the electrochemical performance of Li_3VO_4.

Fig. 6(a) is a low magnification SEM image of the Li_3VO_4 electrode after 100 cycles with charge state, exhibiting a large number of holes on the surface. High magnification SEM image of the cycled electrode is shown in Fig. 6(b), which indicates the electrode consists of a large quantity of nanoparticles with mean size about 100 nm. As seen, these nanoparticles connect with each other, forming a new porous architecture. TEM image provides further insight into the structural details of the cycled electrode. Fig. 6(c) is a TEM image of the cycled Li_3VO_4 electrode, which shows a large number of nanoparticles, and these nanoparticles are composed of smaller particles with size of tens of nanometers. The insert of Fig. 6(c) shows a SAED pattern of the cycled electrode, diffraction rings suggest an amorphous state. Fig. 6(d) is a HRTEM image of the cycled Li_3VO_4 electrode, which suggests the cycled electrode is

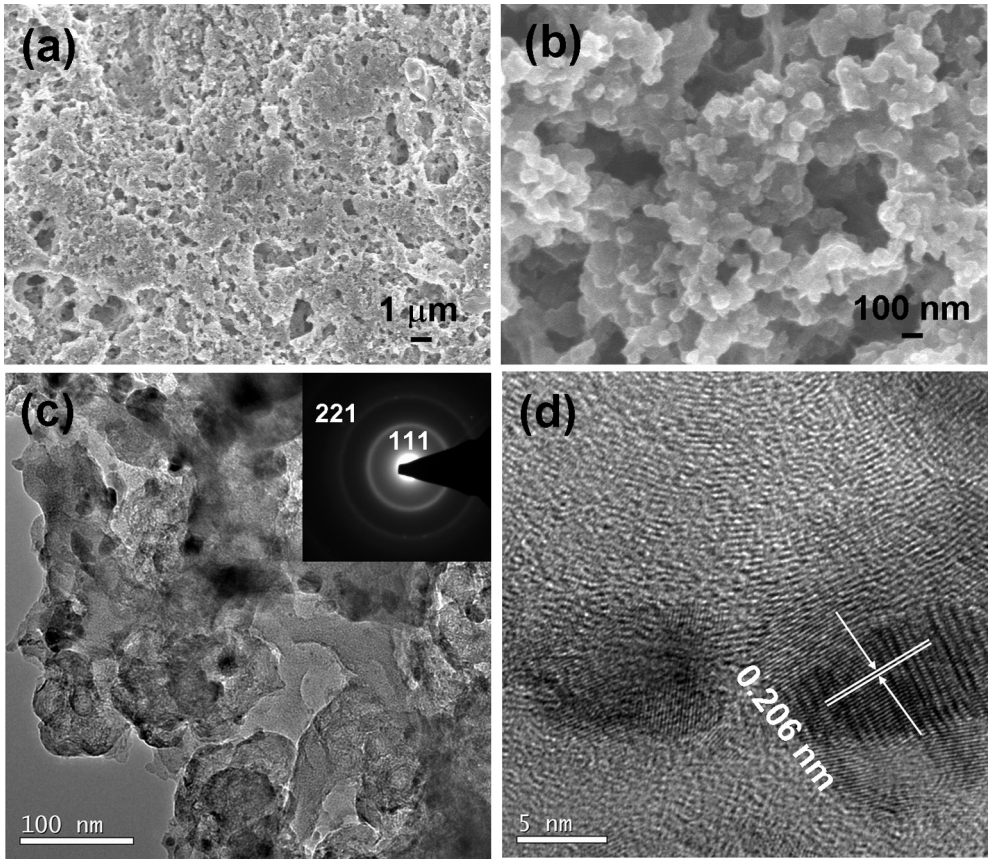

Fig. 6. SEM (a) and (b), TEM (c) and HRTEM (d) images of the Li_3VO_4 electrode after 100 cycles test with charge state. The insert of (c) is a SAED pattern.

amorphous with some crystal grains embedded in the amorphous matrix. The interplanar spacing of the crystal grain is about 0.206 nm, which corresponds to the (220) plane of the orthorhombic Li_3VO_4. Our previous study suggests TMOS that based on a redox reaction mechanism, can realize the morphology variation during charge/discharge test, which can be divided into an electrochemical activation that results in the formation of a large number of nanosized particles and subsequent electrochemical reconstruction that leads to the reassembly of these nanosized particles into new special architecture [28,29]. Here in this study, we are delighted to found a size reduction accompanied by a morphology variation of Li_3VO_4 after cycling test. It means that electrochemical activation and electrochemical reconstruction occurred in Li_3VO_4 electrode, which is a surprised observation in LVOS. The observations are in accordance with the XRD result in Fig. 4 and the proposed charge/discharge mechanism. The reconstructed porous architecture can facilitate the electrochemical reactions between electrode and electrolyte and improve the structure stability of the Li_3VO_4 electrode, resulting in good electrochemical performance.

Fig. 7(a) shows the discharge and charge curves of the Li_3VO_4 electrode at various C rates from 0.2 to 4.0 C. Along with the increase of discharge/charge rate, the discharge potential decreases and the charge potential increases due to kinetic effects of the material, rendering higher overpotential [30]. As shown in the rate capability in Fig. 7(b), the 5th discharge capacity is 408, 358, 311,

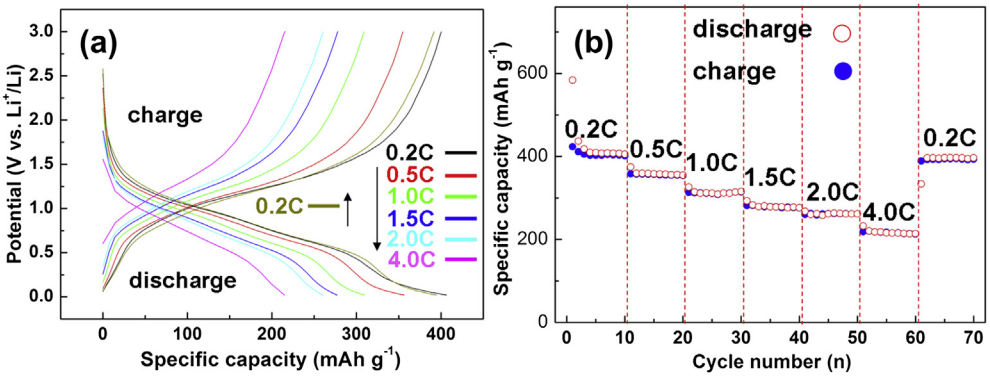

Fig. 7. Representative charge and discharge voltage profiles (a) and capacity retention (b) of Li_3VO_4 electrode at various C rates.

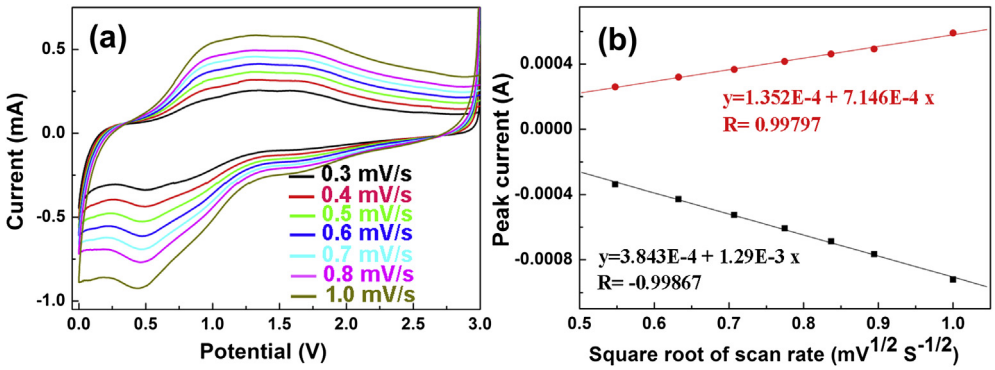

Fig. 8. (a) CV curves of the Li_3VO_4 electrode at different scan rate between 0 and 3 V. (b) Dependence of peak current on the square rate of scan rate for Li_3VO_4 electrode.

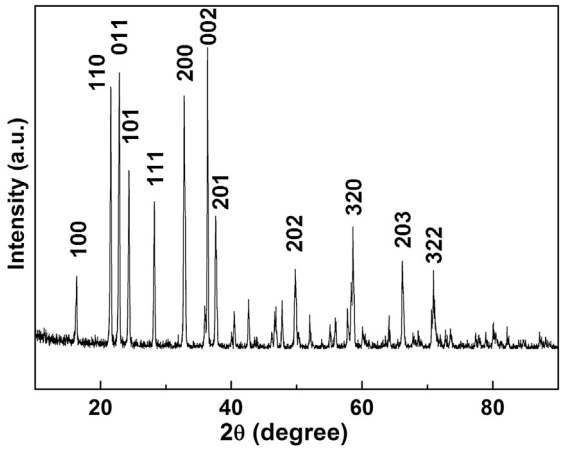

Fig. 9. XRD pattern of the products obtained by annealing the pre-obtained Li_3VO_4 in air atmosphere at 700 °C for 5 h.

279, 262 and 216 mAh g^{-1} at rates of 0.2, 0.5, 1.0, 1.5, 2.0 and 4.0 C, respectively. After that, the discharge capacity can restore to 398 mAh g^{-1} when lowing the discharge/charge rate to 0.2 C. The as-prepared Li_3VO_4 powder electrode shows excellent cycle stability and rate capability, which suggests potential application as anode material for Li-ion batteries.

CV curves of the Li_3VO_4 electrode at scan rates from 0.3 to 1.0 mV s^{-1} are shown in Fig. 8(a). As found, the reduction peak shifts to low potential region along with the increasing of scan rate, whereas the oxidation peaks shift to high potential region, demonstrating the less polarization under a low scan rate. Fig. 8(b) shows the relationship between peak current and square root of scan rate obtained from the experimental data in Fig. 8(a). As shown, both the anodic (delithiation) and cathodic (lithiation) peak currents show linear dependence on the square root of the scan rate from 0.3 to 1.0 mV s^{-1}, suggesting a lithium ion diffusion controlled mechanism in the charge and discharge process [28,31,32]. This observation suggests that electronic conductivity is not a main restriction factor for the electrochemical performance of Li_3VO_4, which imply us that improving the diffuse coefficient of lithium ion is a feasible way to enhance the electrochemical performance of Li_3VO_4.

To obtain Li_3VO_4 with higher purity, the pre-obtained products (500 °C, N_2, 5 h) were further annealed in air atmosphere at 700 °C for 5 h. Typical XRD pattern of the re-annealed products is shown in Fig. 9. As seen, the diffraction peaks located at 16.3°, 21.6°, 22.9°, 24.4°, 28.2°, 32.8°, 36.3°, 37.6°, 49.8°, 58.7°, 66.2° and 70.9° can be observed, which attributed to the (100), (110), (011), (101), (111), (200), (002), (201), (202), (320), (203) and (322) crystal faces of orthorhombic Li_3VO_4 (JCPDS, No. 38-1247). Strong and sharp diffraction peaks suggest that the re-annealed Li_3VO_4 are well crystallized. No diffraction peaks other than those of Li_3VO_4 were detected, indicating high purity of the obtained products.

Fig. 10(a) is a low magnification SEM image of the re-annealed Li_3VO_4, which consists of a large number of microparticles with size ranges from 2 to 10 μm. The mean size of these particles is much bigger than that of the pre-obtained Li_3VO_4, which is due to the crystal growth of Li_3VO_4 under high temperature. For further observation the morphology of the particles, high magnification SEM image of the re-annealed Li_3VO_4 is provided. As shown in Fig. 10(b), these particles are of smooth surface, on which a large number of nanoparticles with size less than 100 nm locate, suggesting a possible Ostwald ripening growth mechanism [33].

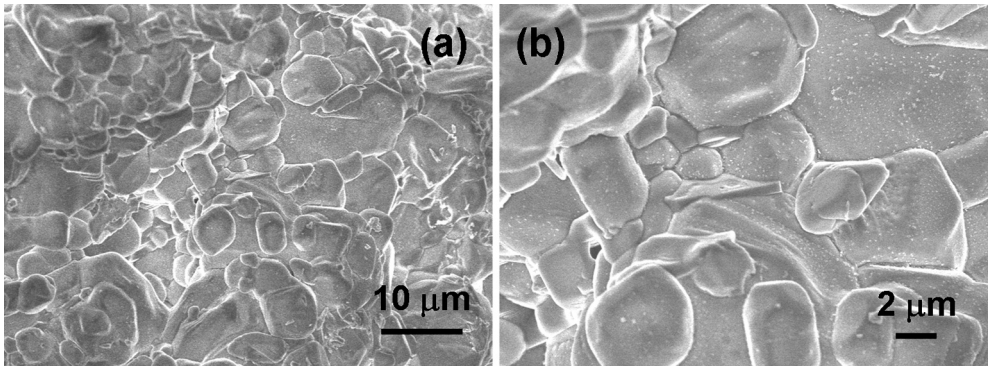

Fig. 10. SEM images of the products obtained by annealing the pre-obtained Li_3VO_4 in air atmosphere at 700 °C for 5 h.

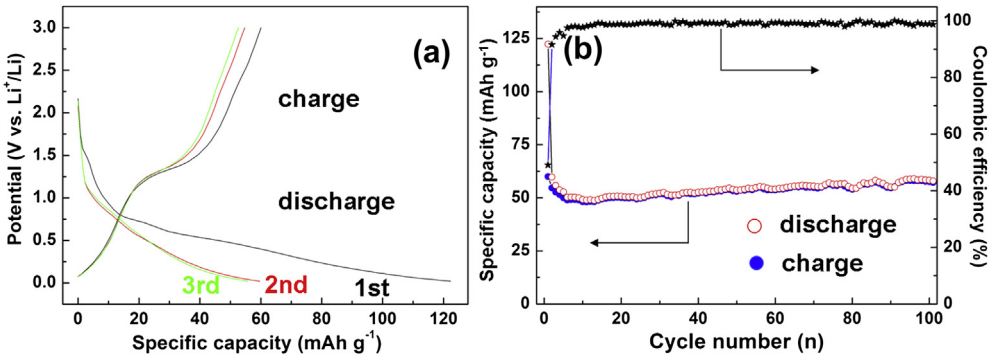

Fig. 11. (a) Initial three charge/discharge voltage profiles of the re-annealed Li_3VO_4 electrode. (b) Capacity retention of the galvanostatic test of the re-annealed Li_3VO_4.

Fig. 11(a) is the initial three charge and discharge voltage profiles of the re-annealed Li_3VO_4 electrode. As seen, when applying an identical current density (comparing with the pre-obtained Li_3VO_4), the electrode shows two sloping potential regions (1.75–0.75 V and 0.75–0.02 V) in discharge curve and a sloping potential region (1.0–1.75 V) in charge curve. The difference between the initial discharge and charge capacity for the Li_3VO_4 electrode is due to the formation of SEI. In addition, the charge/discharge curves differ from these in Fig. 3(a), suggesting different charge/discharge reaction kinetics, which may be relevant to the size and the crystallographic orientation of Li_3VO_4. Fig. 11(b) shows the capacity retention profiles and coulombic efficiency of the Li_3VO_4 electrode. As seen, the discharge and charge capacity are 122.3 and 49.1 mAh g^{-1} in the initial cycle, which decrease along with the increasing of cycle number in the first few cycles, and then gradually reach stable values, being 58.3 and 57.6 mAh g^{-1} after 100 cycles. The first coulombic efficiency of the Li_3VO_4 electrode is 49.1%, which gradually increases in the first few cycles and then reaches a stable value, maintaining a mean value of 98.3% over 100 cycles. It is noticed that the specific capacity of Li_3VO_4 electrode after annealing in air at 700 °C is much smaller than that before annealing, which may be relevant to the size and crystallographic orientation of Li_3VO_4. The bigger the size of Li_3VO_4 is, the lower the diffuse coefficient of lithium ions shows, which leads to worse electrochemical performance of Li_3VO_4. In addition, the annealed sample with bigger size shows lower initial and average coulombic efficiency, which may be due to the amorphization of Li_3VO_4 in lithiation/delithiation process. Based on the obtained experimental results, it can be deduced that the electrochemical performance of Li_3VO_4 may be affected not only by the purity, the particle size and morphology, but also by the inner crystallographic orientation and related lithiation/delithiation process.

4. Conclusions

In summary, Li_3VO_4 was prepared via a facile method and its electrochemical performance as anode for Li-ion batteries was firstly researched. The as-prepared Li_3VO_4 shows good electrochemical performance based on a possible redox reaction mechanism. A novel size decreasing and structure variation of the Li_3VO_4 electrode was observed after cycling, which can be ascribed to an electrochemical activation and subsequent electrochemical reconstruction that induce the formation of a new porous architecture, facilitating the reaction kinetics and improving the electrochemical performance of Li_3VO_4. Further research on optimizing the electrochemical performance of Li_3VO_4 should be done to realize the practical application of this new kind of anode material in Li-ion batteries. Improving the diffuse coefficient of lithium ions may be an effective way to enhance the electrochemical performance of Li_3VO_4.

Acknowledgments

We gratefully acknowledge the financial support from Natural Science Foundation of China (NSFC, 51272128, 51302152, 51302153), Excellent Youth Foundation of Hubei Scientific Committee (2011CDA093), Education Office of Hubei Province (Q20111209) and Open Project of State Key Laboratory Cultivation Base for Nonmetal Composites and Functional Materials (12zxfk08). Moreover, the authors are grateful to Dr. Jianlin Li at Three Gorges University for his kind support to our research.

References

[1] P. Poizot, S. Laruelle, S. Grugeon, L. Dupont, J.M. Tarascon, Nature 407 (2000) 496–499.
[2] G.M. Zhou, D.W. Wang, F. Li, L.L. Zhang, N. Li, Z.S. Wu, L. Wen, G.Q. Lu, H.M. Cheng, Chem. Mater. 22 (2010) 5306–5313.
[3] B. Wang, J.S. Chen, H.B. Wu, Z.Y. Wang, X.W. Lou, J. Am. Chem. Soc. 133 (2011) 17146–17148.
[4] X.W. Lou, D. Deng, J.Y. Lee, J. Feng, L.A. Archer, Adv. Mater. 20 (2008) 258–262.
[5] X.F. Zheng, G.F. Shen, Y. Li, H.N. Duan, X.Y. Yang, S.Z. Huang, H.G. Wang, C. Wang, Z. Deng, B.L. Su, J. Mater. Chem. A 1 (2013) 1394–1400.
[6] S.B. Ni, T. Li, X.L. Yang, Mater. Chem. Phys. 132 (2012) 1108–1111.
[7] Z.G. Yin, Y.H. Ding, Q.D. Zheng, L.H. Guan, Electrochem. Commun. 20 (2012) 40–43.
[8] N.A. Chernova, M. Roppolo, A.C. Dillon, M.S. Whittingham, J. Mater. Chem. 19 (2009) 2526–2552.
[9] L.Q. Mai, X. Xu, L. Xu, C.H. Han, Y.Z. Luo, J. Mater. Res. 26 (2011) 2175–2185.
[10] H.M. Liu, Y.G. Wang, K.X. Wang, E. Hosono, H.S. Zhou, J. Mater. Chem. 19 (2009) 2835–2840.
[11] L. Dai, Y.F. Gao, C.X. Cao, Z. Chen, H.J. Luo, M. Kanehira, J. Jin, Y. Liu, RSC Adv. 2 (2012) 5265–5270.
[12] Y.Y. Liu, E. Uchaker, N. Zhou, J.G. Li, Q.F. Zhang, G.Z. Cao, J. Mater. Chem. 22 (2012) 24439–24445.
[13] L.F. Xiao, Y.Q. Zhao, J. Yin, L.Z. Zhang, Chem. Eur. J. 15 (2009) 9442–9450.
[14] D.H. Sim, X.H. Rui, J. Chen, H.T. Tan, T.M. Lim, R. Yazami, H.H. Hng, Q.Y. Yan, RSC Adv. 2 (2012) 3630–3633.
[15] H.W. Liu, D.G. Tang, Mater. Chem. Phys. 114 (2009) 656–659.
[16] T. Hillel, Y.E. Eli, J. Power Sources 229 (2013) 112–116.
[17] F. Sauvage, V. Bodenez, J.M. Tarascon, K.R. Poeppelmeier, J. Am. Chem. Soc. 132 (2010) 6778–6782.
[18] J.H. Song, H.J. Park, K.J. Kim, Y.N. Jo, J.S. Kim, Y.U. Jeong, Y.J. Kim, J. Power Sources 195 (2010) 6157–6161.
[19] J. Liu, W. Liu, Y.L. Wan, S.M. Ji, J.B. Wang, Y.C. Zhou, RSC Adv. 2 (2012) 10470–10474.
[20] W.J. Wang, H.Y. Wang, S.Q. Liu, J.H. Huang, J. Solid State Electrochem. 16 (2012) 2555–2561.
[21] X.M. Jian, J.P. Tu, Y.Q. Qiao, Y. Lu, X.L. Wang, C.D. Gu, J. Power Sources 236 (2013) 33–38.
[22] S.Q. Wang, J.Y. Zhang, C.H. Chen, J. Power Sources 195 (2010) 5379–5381.
[23] J.Y. Xiang, J.P. Tu, L. Zhang, Y. Zhou, X.L. Wang, S.J. Shi, J. Power Sources 195 (2010) 313–319.
[24] X.H. Wang, X.W. Li, X.L. Sun, F. Li, Q.M. Liu, Q. Wang, D.Y. He, J. Mater. Chem. 21 (2011) 3571–3573.
[25] Z.Y. Wang, F.B. Su, S. Madhavi, X.W. Lou, Nanoscale 3 (2011) 1618–1623.
[26] C. Wang, D.L. Wang, Q.M. Wang, H.J. Chen, J. Power Sources 195 (2010) 7432–7437.
[27] G. Silversmit, D. Depla, H. Poelman, G.B. Marin, R.D. Gryse, J. Electron. Spectrosc. Relat. Phenom. 135 (2004) 167–175.

[28] S.B. Ni, T. Li, X.H. Lv, X.L. Yang, L.L. Zhang, Electrochim. Acta 91 (2013) 267–274.
[29] S.B. Ni, X.H. Lv, T. Li, X.L. Yang, L.L. Zhang, Y. Ren, Electrochim. Acta 96 (2013) 253–260.
[30] S.B. Ni, X.L. Yang, L. Tao, J. Mater. Chem. 22 (2012) 2395–2397.
[31] C.C. Li, X.M. Yin, L.B. Chen, Q.H. Li, T.H. Wang, J. Phys. Chem. C 113 (2009) 13438–13442.
[32] Y.J. Zhu, C.S. Wang, J. Phys. Chem. C 115 (2011) 823–832.
[33] H. Li, Y.F. Liu, M. Guo, R. Zhang, J. Du, Adv. Mater. Res. 374–377 (2011) 1805–1808.